

This is the accepted manuscript of the contribution published as:

Nixdorf, E., Trauth, N. (2018):

Evaluating the reliability of time series analysis to estimate variable riparian travel times by numerical groundwater modelling

Hydrol. Process. **32** (3), 408 – 420

The publisher's version is available at:

<http://dx.doi.org/10.1002/hyp.11428>

Evaluating the reliability of time series analysis to estimate variable riparian travel times by numerical groundwater modelling

Erik Nixdorf^{1,2*}, Nico Trauth³

¹ Department of Environmental Informatics, Helmholtz Centre for Environmental Research-UFZ, Leipzig, Germany

² Faculty of Environmental Sciences, Technical University Dresden, Germany

³ Department of Hydrogeology, Helmholtz Centre for Environmental Research-UFZ, Leipzig, Germany

*Corresponding author

Erik Nixdorf

Department of Environmental Informatics, Helmholtz Centre for Environmental Research, Permoserstrasse 15, D-04318 Leipzig, Germany

Tel. +493412354669

Email: erik.nixdorf@ufz.de

This article has been accepted for publication and undergone full peer review but has not been through the copyediting, typesetting, pagination and proofreading process which may lead to differences between this version and the Version of Record. Please cite this article as doi: 10.1002/hyp.11428

Abstract

The transition zones between rivers and adjacent riparian aquifers are locations of high biogeochemical activities that contribute to a removal of potentially hazardous substances in the aquatic system. The potential of the removal processes depends on subsurface water travel times, which can be determined by using the propagation of electrical conductivity (EC) signal from the river into the riparian aquifer. Although this method has been applied and verified in many studies, we observe possible limitations for the usage of EC fluctuation analysis. Our findings are based on EC time-series analyses during storm events and artificial hydropeaks induced by watermill operations. Travel times derived by cross-correlation analysis were compared with travel times calculated based on backward particle tracking of a calibrated transient numerical groundwater flow model. The cross-correlation method produced only reasonable travel times for the artificial hydropeaks. In contrast, cross-correlation analysis of the EC data during natural storm events resulted in implausibly negative or unrealistically low travel times for the bulk of the data sets. We conclude that the reason for this behaviour is, firstly, the low EC contrast between river and groundwater in connection with a strong damping of the infiltrating river EC signal into the subsurface during storm events. Secondly, the existence of old and less mineralized riparian water between the river and the monitoring well resulted in bank-storage-driven EC breakthrough curves with earlier arrival times and the subsequent estimation of implausible riparian travel times.

Keywords: Riparian zone, Bank storage, Cross-correlation, Electrical conductivity, River-groundwater interaction, Numerical groundwater modelling

1. Introduction

Groundwater and surface water have long been viewed and managed as two separate entities. However, in the vicinity of rivers, interactions between surface water and groundwater create a hydrological continuum. Here, constituents such as dissolved organic matter or nitrate may be retained, transformed or degraded by microbial communities (Findlay, 1995). This natural ability to process substances is essential for the resilience of aquatic ecosystems (Boulton *et al.*, 1998) and helps sustain high quality freshwater (Ray, 2008).

The travel time of infiltrating river water into the subsurface is a crucial factor which controls the solute degradation and transformation processes in the riparian aquifer (e.g. Pinay *et al.* 2009; Zarnetske *et al.* 2012; Boano *et al.* 2014). Travel times to groundwater wells can be determined by measuring breakthrough curves of artificial tracers released in the river water (Davis *et al.*, 1980). Alternatively, natural tracers such as heat and electric conductivity (EC) bearing a fluctuating time series with potentially contrasting values between river water and groundwater can be applied to investigate riparian travel times. A specific advantage of these natural tracers is that they can be recorded at low cost and at high frequency continuously over several years. Although temperature has been established as a widely used natural tracer (Anderson, 2005; Schmidt *et al.*, 2006), EC fluctuations usually show a more advective transport pattern in the subsurface due to their smaller diffusion coefficient, their unambiguous origin and their exclusive transport through the pores (Vogt *et al.*, 2010). Consequently, EC fluctuations propagate over longer distances than do heat fluctuations (Schmidt *et al.*, 2012).

EC fluctuations have been widely used as natural tracers to determine subsurface travel times for a broad range of hydrological conditions, e.g. from the river to a specific location in the groundwater under exclusively losing river conditions (e.g. Vogt *et al.* 2010), to the riparian

zone by strong river stage fluctuations induced by dam operations (Hucks-Sawyer *et al.*, 2009), in streambed sediments of gravel bars (Schmidt *et al.*, 2012; Vieweg *et al.*, 2016) or within river meanders (Osenbrück *et al.*, 2013). Most applications of EC time series were conducted under strong, but not necessarily constant, losing conditions in order to ensure a clear assignment of the propagating EC signal (Dudley-Southern and Binley, 2015). In this study, we demonstrate how alternating hydraulic gradients induced by artificial and natural events, influence variations of EC in the groundwater of a riparian zone of a fourth-order river in central Germany. Spatially and temporally highly resolved measurements of EC time series were performed in both the river and the groundwater of the riparian zone to calculate travel times using the standard cross-correlation method. Subsequently, those analytically derived travel times were compared with travel times computed from backward particle tracking based on the flow field of a calibrated transient groundwater flow model of the site. By doing so, we depict the limitations and the plausibility of EC time series analysis for deriving subsurface travel times in such complex hydrological environments as riparian zones.

2. Methods

2.1 Study Site

The Selke River is a fourth-order stream with a length of 64 km and a catchment size of about 458 km². The river catchment can be roughly divided into two parts: the first within the mostly forested Harz Mountains and the second comprising the agriculturally dominated Northern Harz foreland (Fig. 1a). The study area (51°43'33''N 11°18'40''E) is situated at the transition from the mountains to the lowland of the catchment (yellow rectangle in Fig. 1a). The field site is part of the Terrestrial Environmental Observatories (TERENO) and integrated in a dense, long-term monitoring program (Bogena *et al.*, 2016; Wollschläger *et al.*, 2017). Here, the channel morphology is characterised by slight meanders, pronounced pool-riffle sequences and gravel bars (Trauth *et al.*, 2015) with a long-term mean discharge of 1.54 m³/s whereas the conditions of incipient inundation of the floodplain is marked by river discharges of more than 25 m³/s at the study site. During periods with a discharge below 1 m³/s (typically June to October) a water mill located 2 km upstream of the field site temporarily stores and releases river water causing river stage rises of up to 15 cm within less than 30 minutes. These fluctuations occur two to three times per day on weekdays.

The aquifer consists of alluvial sand and gravel deposits up to a depth of 10 m below surface. The base of this highly permeable aquifer is a silty clay layer, which acts as an aquitard. The top of the aquifer is covered by an alluvial loam layer of up to 1 m thick, which inhibits fast infiltration of atmospheric water into the aquifer. Depth to groundwater is less than 1.2 m below ground surface leading to predominantly unconfined conditions. Further water bodies, like small tributaries or springs do not exist at the field site. Although gaining and losing conditions alternate along the Selke River, losing conditions predominate at the local field site representing an infiltration of river water into the riparian aquifer.

2.2 Data collection

Six monitoring wells of 1" diameter were installed in the riparian zone of the Selke River with a depth of 4 m and a distance from the river ranging from 10 to 50 m (Fig. 1b). The wells were drilled by direct push technology and are screened from 3 to 4 m below ground. After the drilling and installation of the wells, the space between outer well tube and soil in the unsaturated zone (alluvial loam) was filled with bentonite in order to avoid infiltration of rainwater instead of groundwater. A cap at the top of the well prevented direct rain input into the well, but still allowed well venting. The exact positions of the wells were determined by a differential GPS in combination with a laser tachymeter (*Trimble GPS R8*). Furthermore, triangulation was used to determine a detailed slope of the river water level at the study site.

The wells F1-F4 were equipped with data loggers (*Solinst LTC Levelogger Junior*), which were able to measure specific electrical conductivity at 25°C with an accuracy of $\pm 20 \mu\text{S}/\text{cm}$ and the water level by applying hydrostatic pressure equation reaching an accuracy of $\pm 0.5 \text{ cm}$. Two additional data loggers (*Solinst Levelogger Edge*) were installed in the wells F5 to F6 in order to measure water level. The latter two were replaced by *Solinst LTC Levelogger Junior* two months after the start of the monitoring period. All loggers were located at the middle of the screened well sections at a depth of 3.5 m below surface. To obtain detailed river stage and EC signal of the river water a *Solinst LTC Levelogger Junior* was installed at the stream bed (location "FF" in Fig. 1b) next to the wells. Water level measurements from the loggers were converted to hydraulic heads by air pressure correction. Local rainfall data with a resolution of 30 minutes was measured by a weather station at a distance of about 2 km from the field site.

The measurement period of the loggers comprised a period of almost five months with a temporal resolution of 10 minutes. The chosen investigation period allowed investigating the

impact of alternating hydraulic gradients imposed by the influence of both the upstream water mill and natural storm events on the flow field in the riparian zone. In total, we focused our investigations on the eight highest natural storm events and 16 smaller mill-induced events during this period.

After the measurement period of the EC loggers, three natural gradient salt tracer tests were conducted in the northern riparian zone in order to determine flow velocity and direction of the groundwater in the riparian aquifer. For each test we injected 200 litres tracer volume into well Fx (Fig. 1c) over a period of 40 minutes. The EC concentration of the tracer was about 130,000 $\mu\text{S}/\text{cm}$. At a distance of 12 m to the injection well Fx, 15 monitoring wells (Ft1-Ft15) were equipped with loggers recording EC concentrations in the lower part of their screened section at a depth of 4 m. The first salt tracer test was conducted during the falling limb of a storm event at a river discharge of about 3.8 m^3/s . When the pre-test EC values were reached after 14 days, the second salt tracer was conducted at low to moderate river discharges of about 0.9 m^3/s . A third tracer test took place under summer base flow conditions (0.2-0.3 m^3/s).

2.3 Analysis of EC time series

Over the last decades, many mathematical approaches such as cross-correlation (Sheets et al., 2002; Vogt et al., 2009), non-parametric deconvolution (Cirpka et al., 2007; Liao et al., 2014) and dynamic time warping (Schmidt et al., 2012) have been developed and applied to extract riparian travel times from measured EC time series. However, for this study we chose a standard cross-correlation based approach, which is a very common, simple and comprehensible method to estimate the association between events in two time series (Vieweg et al., 2016).

The cross-correlation method examines the movements and proximity of alignment between two statistically independent time series $X(t)$ and $Y(t)$ by shifting one series $Y(t)$ by a number of time steps k and summing the multiplied pairs of values to generate the cross-correlation function (Kresic, 1997). Transferred at the analysis of EC fluctuations, $X(t)$ is defined as the EC time series of the river (EC_{River}) and the temporary shifted signal $Y(t)$ refers to the EC time series measured in the corresponding groundwater wells (EC_{GW}). A measure of the strength of the correlation is given by a normalised correlation coefficient (ρ) which depends on the time lag k .

$$\rho(k) = \frac{\sum_{i=1}^n EC_{\text{River}}(t_i) \cdot EC_{\text{GW}}(t_i + k)}{\sqrt{\sum_{i=1}^n (EC_{\text{River}}(t_i))^2 \cdot \sum_{i=1}^n (EC_{\text{GW}}(t_i + k))^2}} \quad (1)$$

Since the signals of EC time series in river and riparian groundwater are non-stationary, the time series were subdivided into single sets of shorter time series, so-called “windows”, which were subsequently used for the cross-correlation (e.g. Vogt *et al.*, 2010). The selection of the window size is of great importance as an overly short window size will decrease result reliability, but an overly long window will tend to decrease the sensitivity of the correlation coefficient on the actual investigated event (Razavi *et al.*, 2015). Considering our particular data, we decided to divide the entire time series into intervals covering the time between the starting points of successive events in the river. All EC time-series sets were detrended by subtracting their respective mean EC value and dividing it by the variance in order to enhance the signal and to improve signal stationarity (Horvatic *et al.*, 2011; Delleur *et al.*, 1976).

For the situation of the storm events, extended periods between successive events of up to a month resulted in considerable large window sizes including signal variations from different sources. To reduce these effects, we did not calculate the advective travel time of infiltrating

river water to the groundwater well from the time shift k_{\max} which was associated with the maximum correlation coefficient of each time series window (Vogt *et al.*, 2010), but by adapting the peak-picking algorithm developed by Boker *et al.* (2002). Assuming that a response between both signals occurs relatively shortly after the start of each event, this algorithm delineates the advective travel times by finding local peaks of the cross-correlation coefficient centred in a local region closest to a time lag of zero. For more details about the method, the interested reader is referred to Boker *et al.* (2002).

2.4 Groundwater model and particle tracking

A two-dimensional numerical groundwater model was developed to simulate the transient behavior of the groundwater flow field in the study area using the numerical code OpenGeoSys v5.7. OpenGeoSys is a scientific open-source project for the development of numerical methods to simulate thermo-hydro-mechanical-chemical (THMC) processes in porous and fractured media based on the finite element method (Kolditz *et al.*, 2012). It has been widely used in previous studies for simulating groundwater flow (e.g. Sun *et al.*, 2012; Nixdorf *et al.*, 2017).

The study area was transformed into a two-dimensional triangular unstructured mesh (Fig. 2) consisting of about 36,000 elements using the finite element mesh generator Gmsh (Geuzaine and Remacle, 2009). The domain size was selected based on preliminary test runs in order to avoid an impact of the lateral no-flow boundary conditions on the local flow field at the test site. Due to refinements near the wells and the river, element edge lengths vary from a few centimetres to up to 20 m at the outer boundary of the modelling domain (Tab. 1). The hydraulic conductivity in the domain was assumed homogeneous and isotropic. A porosity value of 0.3 was selected which is a typical value for fluvial sediments (Fetter, 2013; Gelhar

et al., 1992) and has been applied for other numerical and analytical studies at the field site (Trauth *et al.*, 2015; Vieweg *et al.*, 2016; Trauth and Fleckenstein, 2017).

The spatial-temporal distribution of hydraulic heads in the river was simulated by applying a time-variant head boundary on all mesh nodes belonging to the 7-m-wide and 350-m-long area of the model representing the river. The time-variant head boundaries were calculated based on measured transient river stage and riverbed topography at several locations along the river reach. Also, time-variant head boundaries were set at the upstream and downstream boundaries of the model domain, where ambient groundwater is flowing into and out of the domain, respectively (green and brown lines in Fig. 2). They were parameterized by the Dupuit equation (Kresic, 1997) for unconfined flow based on the transient river stage at the upstream and downstream river nodes as well as the hydraulic head at the edges of the domain (visualised as grey triangles in Fig. 2). No-flow boundaries were used along the base, the top, the downstream-left, and downstream-right boundaries of the model.

For the calibration of the transient groundwater flow model three metrics derived from the three natural gradient salt tracer tests were used as target parameters, which describe the main characteristics of the real groundwater flow field: i) The mean advective transit time of the tracer, ii) the location of the centre of the tracer mass, and iii) the groundwater heads in the wells Ft1 to Ft15. For ii) and iii) the value at the time of mean advective tracer transit was used. Forward advective particle tracking was applied to the computed transient flow fields of the groundwater flow simulations by using an algorithm implemented in MATLAB®. Similar to the location of the real tracer test injection, particles were released at Fx and the subsequent movement of the particle was calculated based on the flow fields.

As calibration parameters the hydraulic conductivity as well as the specific heads at the edges of the domain were used. For the latter ones, we defined the depth to groundwater at

maximum and minimum discharge as the actual calibration parameter and linearly interpolated values in between during the transient calibration process. Furthermore, similar depths to groundwater were assigned to all domain edges for each specific value of river discharge. The calibration process was done using the model-independent parameter estimation code PEST (Doherty, 2015) to automatically calibrate the model.

After successful calibration of the groundwater model, subsurface travel times from the river to the monitoring wells during the eight storm events were calculated by using backward-particle tracking. In general, the same algorithm as was applied to the advective forward-particle tracking was applied here but using instead reversed velocity vectors from the groundwater flow model. The starting time for the backward particle tracking for each storm event was estimated by using the time of EC minima in the river plus the respective travel time to each well calculated by the cross-correlation to ensure result comparability between both methods. The final position of each backward particle path was reached when the particle entered a river element. In cases where the simulated particles did not reach the river within the measurement period, linear extrapolation was applied on the existing particle path to compute the subsurface travel times.

3. Results

3.1 River hydrology and EC at the field site

Discharge in the Selke River showed a mean of $1.69 \pm 1.03 \text{ m}^3/\text{s}$ during the observation period. Occasional rain events and the snowmelt at the beginning of February 2014 caused numerous storm events in the Selke River with discharge up to $7.2 \text{ m}^3/\text{s}$ and corresponding water level variations at the river logger position of 0.6 m (Fig. 3a). During the first two weeks of the observation period where river discharges were down to $0.18 \text{ m}^3/\text{s}$, the upstream water mill periodically triggered a mean fluctuation in discharge of about $0.1\text{-}0.2 \text{ m}^3/\text{s}$. The increased river discharge in autumn made water storage for mill operation unnecessary.

EC in the Selke River ranged between $228 \text{ }\mu\text{S}/\text{cm}$ and $570 \text{ }\mu\text{S}/\text{cm}$ with a mean of $306 \pm 58.4 \text{ }\mu\text{S}/\text{cm}$ within the observation period. Significant storm events caused a drop in EC between $30 \text{ }\mu\text{S}/\text{cm}$ and $200 \text{ }\mu\text{S}/\text{cm}$ whereas the water mill operation induced EC fluctuations of about $30 \text{ }\mu\text{S}/\text{cm}$ (Fig. 3b/c). The relationship between discharge and EC can be described by a negative power-law-relationship (Fig. 3d), which is presumably caused by a dilution of river water during an increasing contribution of direct runoff during floods (e.g. Sandén et al., 1997). Hence, fluctuations in discharge had a larger effect on EC variations during periods of low discharge conditions (baseflow) whereas during high discharge the river EC did not fall below $230 \text{ }\mu\text{S}/\text{cm}$. The scattering of the data points in Fig. 3d is presumably related to a typical hysteresis effect between river discharge and ion mobilization and dilution effects, affecting EC (Evans and Davies, 1998). Consequently, EC values were lower during the falling limb of event's hydrograph than in the rising limb under similar discharges.

3.2 Spatial and temporal variability of groundwater levels and EC distribution

In general, average water level of the Selke River was higher than the groundwater at the near-stream wells F3 and F4, showing that losing conditions occurred for the entire observation period (Fig. 4a/c). In the northern riparian zone, average groundwater levels at the inner meander bank increased from F3 to F2 to F1. In contrast, groundwater levels further decreased at the southern side of the riparian zone with increasing distance from the river towards well F6 (Fig. 4a/c).

Groundwater table variations strongly corresponded to changes of river stage. Event-driven fluctuations of river water level propagated slightly damped to the six monitoring wells, which all showed maximum variations in water level of about 0.5 m (see Fig. 4c). Further, considering both the absence of springs in the area and of a direct rainwater input, this implied that riparian groundwater hydraulics at the field site were controlled to a large part by river stage variations. However, water level fluctuations showed a time lag of 2 h to 8 h to those of the river stage, depending on the magnitude of the storm event and the well distance from the river.

Observed EC in all monitoring wells exceeded the EC values of the Selke River during the entire monitoring period (Fig. 4b/d). The increase in EC in the monitoring wells with increasing distance to the river indicated a mixing with ambient groundwater which had EC values of 1,300 to 1,500 $\mu\text{S}/\text{cm}$ (Vieweg *et al.*, 2016). This occurrence of a continuous mixing zone in near-stream aquifers has been observed in many studies on riparian zone hydrochemistry (e.g. Vidon, 2012; Duval and Hill, 2006).

In general, EC concentrations are higher in the southern aquifer because of a significantly larger agricultural area draining into the river. In comparison, the sub-catchment boundary at

the northern aquifer is reached within 700 m from the river. Also, different farming cultivation and fertilization may lead to the differences in absolute EC values.

In contrast to water level fluctuations, dynamic changes in river EC were not always observable in the monitoring wells, in particular in well F1 and F6, which were located farthest from the river. The largest absolute range of EC values was measured in the wells F2 and F3 located in the inner meander bank (Fig. 4d).

3.3 Observed and simulated flow path and velocity dynamics during the tracer tests

The analysis of the salt tracer tests revealed that most of the tracer mass was detected in the monitoring wells Ft2 and Ft3 for all river discharge conditions. However, we observe that with increasing river discharge the main groundwater flow direction shifted slightly towards the north, away from the general river course. Calculated mean advective groundwater flow velocities were between 2.44 and 3.66 m/day, showing an increasing velocity with decreasing river discharge.

The performance of the calibrated numerical model was assessed by calculating the root-mean-square error (RMSE) between the observed and the simulated values of the three target parameters. Overall, the comparison with the measurement showed that the calibrated groundwater flow model was able to resemble all three target parameters for each tracer test with a high accuracy (Fig.5a-c).

The calibrated groundwater flow model allowed visualising the effect of river morphology and changing hydraulic conditions on the riparian flow conditions during the tracer tests (Fig. 5d-f). Groundwater velocities were higher in the southern riparian zone, indicating stronger losing conditions than in the northern riparian zone. Particularly in the southern riparian aquifer, subsurface velocities further increased with decreasing river discharge. In addition, groundwater velocities in the riparian zone varied along the pool-riffle sequences of

the river showing higher flow velocities in the vicinity of areas with steeper river slope and vice versa.

Similar to the hydraulic head obtained from the time series data, the groundwater model demonstrated that losing conditions prevail along the investigated river section. Only at very narrow zones, a local hyporheic zone (flow path that exit and enter the river) developed in the northern riparian zone at the inner side of the meander bank (Fig 5d-f, at $x=80$, $y=30$). The river water that reached the northern monitoring wells F1 and F2 originates from river sections upstream of the pool section with travel distances of about 60 and 40 m, respectively.

3.4 Travel times during water-mill-induced events

The propagation of the water-mill-induced EC fluctuations was only detected in well F4, which was located closest to the river bank. The cross-correlation of the complete EC time series of the river and well F4 during the water mill operation period resulted in a mean advective travel time of 2.8 h (Fig. 6a). According to the corresponding maximum correlation coefficient about 60 % of the EC variations in well F4 can be explained by variations of the river EC signal (Fig. 6b). River EC fluctuations with small amplitude which were not caused by the water mill operations did not propagate into well F4 (red circle in Fig 6a.). In addition, EC fluctuation with very short duration, e.g. between the events #3 and #4, could not be detected in the monitoring well.

Similar values of advective travel times τ of 2.7 ± 0.7 h and correlation coefficients ρ of 0.76 ± 0.11 (Tab. 2) were calculated by applying the cross-correlation to the 16 individual mill events (light blue and brown triangles in Fig. 6a). Since the travel times of the 16 individual events were different, the cross-correlation applied over the entire time series lead to lower correlation coefficients. At 58.6 ± 0.3 h, travel times to well F4 estimated by the backward-

particle tracking method were about one magnitude higher than the cross-correlation estimates (see discussion).

3.5 Travel times during river storm events

The standardized EC signal of the eight storm events showed very different responses in each of the four monitoring wells (Fig. 7). In the most distant well F1, EC fluctuations were detected only during storm event #3, which showed the highest discharge within the observation period. In contrast, well F2, which is located halfway between F1 and the river, showed EC variations for each storm event.

Positive travel times could only be estimated for about 55 % of all investigated time series data pairs using the cross-correlation method. Beside other effects, a decreasing EC was recorded in the monitoring well F3 and F4 earlier than the river for several events. This observed phenomenon is incompatible with the assumption of standard EC time series analysis methods that the EC fluctuations of the river water level propagate within a specific time lag into the riparian aquifer. Consequently, the application of the cross-correlation method to these data sets lead to negative travel times which are physically implausible (Tab. 3).

For the numerical backward-particle tracking, calculated mean travel times to the wells for the eight storm events were 508 ± 5.1 h for well F1, 482 ± 5.7 h for well F2, 215 ± 1.4 h for well F3 and 49 ± 1.1 h for well F4. The order of the estimated mean travel times to each well matches the order of associated flow path lengths in the riparian aquifer according to the numerical groundwater flow model (Fig. 5d-f). In contrast, differences in travel times to a single well during different storm events were relatively small.

For the cross-correlation estimates, derived positive travel times varied in a broad range for each event and for each well (Tab. 3). Calculated positive subsurface travel times between the

river and well F4 were similar to the previous calculation for the mill-induced events. Surprisingly, the estimated travel time to well F1 (during event #3) was in a similar range although the calculated flow path's length from the river to F1 was around 10 times longer than to F4. Additionally, travel times to F1 were around one to 1.5 orders of magnitude lower than the travel times to well F2 and F3. In turn, those short travel times to the distant well F1 would require a much higher groundwater flow velocity towards F1 than were estimated in the tracer tests and the calibrated groundwater model. Furthermore, the quantity of the cross-correlation coefficients ρ decreased with increasing distance to the river, meaning the highest coefficients were found for well F4, lower coefficients for well F2, and finally lowest cross-correlation coefficient for well F1. This spatial change of the coefficients indicates that the impact of storm events on riparian groundwater decreased with increasing distance from the river.

In summary, there were effects of varying strength and impact of storm events on riparian groundwater EC. As mentioned above, a considerable amount of data sets used for travel time estimation by the cross-correlation method lead to hydrologically unrealistic results, showing negative or extremely short travel times. For the latter ones, an extremely high groundwater flow velocity would be needed to produce the observed EC fluctuations. A good criterion to prove the reliability of estimated (positive) subsurface travel times calculated by cross-correlation is to compare them with the travel times derived from the numerical groundwater model in combination with particle tracking.

4. Discussion

Estimated travel times of the cross-correlation method and the groundwater flow model showed discrepancies between one to two orders of magnitude (Fig. 8). Particularly for well F1 and F2 simulated travel times were up to 720 times higher than those estimated by the cross-correlation. Although even for well F4 resulting riparian travel times differ by a factor from 10 to 50 between both estimation methods, the detection of consecutive mill-induced EC fluctuation confirmed that the positive cross-correlation estimates are plausible for this well (Sawyer et al, 2009). The overestimation of riparian flow times to well F4 by the groundwater flow model may be related to the known impact of locally increased groundwater flow velocities by preferential flow paths due to high conductive layers (Beven and Germann, 1982; Hester *et al.*, 2017) or along tree roots in the riparian zone (Bargués Tobella *et al.*, 2014). However, it is very unlikely that those strong discrepancies between the two methods can be explained exclusively for all wells by heterogeneity in the subsurface aquifer, particularly considering that the groundwater flow model was calibrated to the salt tracer data at the northern riparian zone.

Therefore, we hypothesize that several EC breakthrough curves in the groundwater wells cannot be attributed to a direct inflow of river water into the well during an event. Instead, the EC breakthrough curves observed in the wells are presumably related to pre-stored groundwater in the riparian aquifer that moves towards the well and hence produces bank-storage-driven EC breakthrough curves because of its different ion concentration.

This effect can be explained by the interplay between changing hydraulic gradients during storm events and the dynamics of the spatial distribution of EC in river water and the riparian zone (Fig. 9). In general, the EC distribution in the riparian zone (time T1 in Fig. 9) is the result of the long and ongoing mixing process of river water and groundwater in the riparian aquifer (Engdahl *et al.*, 2016; McCallum and Shanafield, 2016), conditions that were also

confirmed by our data (see Fig. 4). Rising river stages of an event temporally shifts the hydraulic system towards stronger losing conditions, which favours a stronger infiltration of river water into the riparian aquifer. Simultaneously, the subsurface water, which already existed in the interstice between the river and the well, is pushed towards the monitoring wells (Time T2 in Fig. 9). As a result, the ion concentration of the water that reaches the well has a higher river water composition and hence, leads to lower EC in the well. This effect appears as a breakthrough curve in the EC time series and can be observed during several events in our dataset (Fig. 7).

Furthermore, the hydraulic head gradient between river and well might not be strong enough to transport the river EC signal to the well permanently, especially when the well is located distant to the river (e.g. well F1 in our dataset). During a storm event, the strongest losing conditions occur ahead of the peak discharge. Similarly, the weakest losing conditions can be found in the aftermath of the peak where discharges were still relatively high (e.g. Chen and Chen 2003). Additionally, changes in river discharge could be detected earlier than the corresponding EC changes (Fig. 3) due to the push of water with a different EC signal in front of the event's flood wave (Krein and De Sutter, 2001; Kirchner, 2003).

Consequently, the decreasing river EC signal propagated into the riparian aquifer during decreasing intensity of losing conditions (Time T3 in Fig. 9), which leads to an enhanced mixing of river water due to the countervailing inflow of ambient groundwater into the riparian zone (e.g. Duval and Hill, 2006; Vidon, 2012). Furthermore, the strength of mixing processes may vary considerably with hydrogeological site conditions (e.g. Hester *et al.*, 2013; Gomez and Wilson, 2013). For example, dispersivity might play a critical role on mixing at the meander scale as higher dispersivity values increase the contribution of ambient groundwater along the riparian flow paths (Gomez *et al.*, 2012). The enhanced mixing contributes to the dampening of the propagating EC variation in the riparian aquifer (Time T4

in Fig. 9), particularly when considering that river EC variations are relatively small for many of the storm events.

In summary, the above mechanism creates natural EC signals in the riparian groundwater that upon first view may bear the potential for calculating riparian travel times, but lead to implausible and erroneous results when applying cross-correlation methods. This further reveals that the occurrence of variations in river EC and its propagation into the subsurface due to losing conditions can only be regarded as a necessary but not sufficient condition that riparian travel times can be calculated based on EC time series analysis.

As a further condition, we hypothesize that specific event characteristics, namely the change of river water level and the corresponding change of solute concentration, have a major impact on the transmissibility of EC fluctuations within the riparian zone. In detail, we assume that a steep hydraulic gradient caused by a rapid increase in river stage and rapid infiltration of river water with a high EC contrast supports the detectability of propagating EC fluctuations in the aquifer and vice versa. In order to proof this hypothesis, we compare the slope of the river hydrograph on the rising limb with the corresponding (negative) slope of the EC signal. In Fig. 10 the two slopes are plotted against each other for both the natural storm events and the artificially induced mill events as well as for three EC fluctuations in the river. The latter ones occurred over the weekend when the water mill was not operating (red circle in Fig.6) and measured variations of river EC were not observable in well F4.

Clearly, in the case of the 16 mill-induced events, the hydraulic and chemical gradients were about one magnitude higher compared to the storm events (Fig. 10). Presumably, the different peak shape between a mill-induced event and a natural storm event is an effect of different solute mobilisation processes. The mill-induced peaks are created at one location (the mill) which consequently leads to steep slopes in both the hydrograph and the chemograph. In

contrast, the natural peak is broader showing less steep slopes because it contains the sum of different water flux and solute signals along the entire river reach upstream of our site. On the other hand, the EC fluctuations that do not propagate into the aquifer during inactive mill operations showed a similar range of chemograph slopes to the natural storm events but significantly smaller hydrograph steepness. This clearly indicates that the strength of losing conditions is of great importance for signal propagation. However, among the storm events, a simple relationship that higher gradients lead to more reliable cross-correlation estimates (see Tab. 3) could not be obtained.

To find out whether a certain threshold needs to be exceeded to ensure a propagation of river EC fluctuations to the well, we compared our results with the slope characteristics of four studies at different field sites where both water level and river EC signal in the river and its propagation into the riparian aquifer was recorded (Fig. 10). For the dataset of Sheets et al. (2002), the cross-correlation method was successfully applied which coincides with steep slopes of both the hydrograph and chemograph similar to the mill-induced events at our field site. Welch et al. (2013) obtained riparian travel times for similar slope characteristics under natural flow conditions, although in their data, infiltration was artificially induced by pumping wells, which supported the EC signal propagation (similar to the studies on EC propagation at the Thur field site by Diem et al, (2013) and Vogt et al (2010)). Similarly, in the dataset of Sawyer et al. (2009), the propagation of each EC fluctuation induced by the dam release events can be traced individually towards the riparian zone. Here, the observed hydrograph and chemograph slopes of each dam release event are in the range of slopes where the cross-correlation method would be an appropriate method. In contrast, adding the data of Welch et al. (2014) to Fig. 10, a significantly lower slope in the chemograph is observable. Interestingly, in Welch et al. (2014), the authors conclude that their travel time estimation method did not lead to plausible travel times in the studied aquifer and account

this to the lack of a heterogeneous setup. However, it is possible that their observed mismatch is based on pre-stored groundwater in the riparian aquifer that is transported towards the well during the event and creates the aforementioned bank-storage-driven EC breakthrough curves. Hence, we think that comparing the hydrograph and chemograph slopes of a recorded event could be a helpful tool to decide whether calculating reliable travel times is possible using time series analysis methods.

5. Summary and conclusions

In this study we investigated riparian travel times by applying windowed cross-correlation to the propagation of EC fluctuations in the riparian zone induced by upstream water mill operation or natural storm events. Although the hydraulic system was constantly losing, the magnitude of hydraulic gradients varied with changing river discharges. For the mill-induced events, the method was successfully applied and successive EC fluctuations with a plausible mean travel time of about 170 min could be individually detected in the well closest to the river (F4). In contrast, for most of the EC fluctuations during storm events, although major efforts were made to improve the signal quality, windowed cross-correlation did not lead to plausible travel times. For more than 40 % of the data sets the calculated travel times were negative which is hydrologically implausible. For the EC data sets that lead to positive travel times, we compared the derived travel times with simulation results of a numerical groundwater model in combination with particle tracking. As differences in estimated travel times were up to two orders of magnitude between the two methods, we conclude that some EC fluctuations detected in the well cannot be attributed to a direct infiltration of river water.

We argue that two effects primarily account for these disparities. Firstly, the river water does not reach the well because hydraulic and chemical gradients were insufficient and mixing of the infiltrating river water with groundwater in the aquifer dampened the EC signal.

Secondly, pre-existing groundwater in between the monitoring well and the river with a lower ion concentration infiltrates into the well during high river stages and produces “bank-storage-driven EC breakthrough curves” in the well that lead to implausible time lags in the cross-correlation method.

To distinguish whether EC time-series data are suitable to estimate travel times in the riparian aquifer, we propose a method, which is based on analysing the slope of the rising river stage and the corresponding falling river EC of an event. Based on our data and four external data sets, we conclude that if induced infiltration (e.g. by riverbank filtration) to wells is absent, both high hydrograph and chemograph slopes are an important prerequisite for the successful application of the event-based cross-correlation of EC fluctuations. Consequently, our findings show that the reliability of estimating subsurface travel times using these methodology, although constantly under losing conditions, may be limited. This has implications for future studies using EC fluctuations to investigate subsurface travel times. Hence, in order to avoid misinterpreting derived travel times, the origin of the EC signal in the riparian zone wells has to be known, which requires, in turn, detailed knowledge of the hydrology of the river-groundwater interface.

Acknowledgements

The research was supported by TERENO (Terrestrial Environmental Observatories) and by the Helmholtz Centre for Environmental Research, Leipzig (UFZ). We thank Toralf Keller for technical support and Niklas Gassen for the initial tracer test planning. The constructive comments of two anonymous reviewers are also gratefully acknowledged.

Accepted Article

References

Anderson MP. 2005. Heat as a ground water tracer. *Ground water* **43** (6): 951–68 DOI: 10.1111/j.1745-6584.2005.00052.x

Bargués Tobella A, Reese H, Almaw A, Bayala J, Malmer A, Laudon H, Ilstedt U. 2014. The effect of trees on preferential flow and soil infiltrability in an agroforestry parkland in semiarid Burkina Faso. *Water Resources Research* **50** (4): 3342–3354 DOI: 10.1002/2013WR015197

Beven K, Germann P. 1982. Macropores and water flow in soils. *Water Resources Research* **18** (5): 1311–1325 DOI: 10.1029/WR018i005p01311

Boano F, Harvey JW, Marion A, Packman AI, Revelli R, Ridolfi L, Wörman A. 2014. Hyporheic flow and transport processes: Mechanisms, models, and biogeochemical implications. *Reviews of Geophysics* **52** (4): 603–679 DOI: 10.1002/2012RG000417

Bogena H, Borg E, Brauer A, Dietrich P, Hajnsek I, Heinrich I, Kiese R, Kunkel R, Kunstmann H, Merz B, et al. 2016. TERENO : German network of terrestrial environmental observatories. *Journal of large-scale research facilities* **52**: 1–8 DOI: <http://dx.doi.org/10.17815/jlsrf-2-98>

Boker SM, Xu M, Rotondo JL, King K. 2002. Windowed cross-correlation and peak picking for the analysis of variability in the association between behavioral time series. *Psychological methods* **7** (3): 338–355 DOI: 10.1037/1082-989X.7.3.338

Boulton AJ, Findlay S, Marmonier P, Stanley EH, Valett HM. 1998. the Functional Significance of the Hyporheic Zone in Streams and Rivers. *Annual Review of Ecology and Systematics* **29** (1): 59–81 DOI: 10.1146/annurev.ecolsys.29.1.59

Chen X, Chen X. 2003. Stream water infiltration, bank storage, and storage zone changes due to stream-stage fluctuations. *Journal of Hydrology* **280** (1–4): 246–264 DOI: 10.1016/S0022-1694(03)00232-4

Cirpka O a., Fienen MN, Hofer M, Hoehn E, Tessarini A, Kipfer R, Kitanidis PK. 2007. Analyzing bank filtration by deconvoluting time series of electric conductivity. *Ground Water* **45** (3): 318–328 DOI: 10.1111/j.1745-6584.2006.00293.x

Davis SN, Thompson GM, Bentley HW, Stiles G. 1980. Ground-Water Tracers — A Short Review. *Ground Water* **18** (1): 14–23 DOI: 10.1111/j.1745-6584.1980.tb03366.x

Delleur JW, Tao PC, Kavvas ML. 1976. An evaluation of the practicality and complexity of some rainfall and runoff time series models. *Water Resources Research* **12** (5): 953–970

Diem, S., Renard, P., Schirmer, M., 2014. Assessing the effect of different river water level interpolation schemes on modeled groundwater residence times. *J. Hydrol.* 510, 393–402. doi:10.1016/j.jhydrol.2013.12.049

Doherty J. 2015. *Calibration and Uncertainty Analysis for Complex Environmental Models*. Watermark Numerical Computing: Brisbane, Australia.

Dudley-Southern M, Binley A. 2015. Temporal responses of groundwater-surface water exchange to successive storm events. *Water Resources Research* **51** (2): 1112–1126 DOI: 10.1002/2014WR016623

Duval TP, Hill AR. 2006. Influence of stream bank seepage during low-flow conditions on riparian zone hydrology. *Water Resources Research* **42** (10): 1–12 DOI: 10.1029/2006WR004861

Engdahl NB, McCallum JL, Massoudieh A. 2016. Transient age distributions in subsurface

hydrologic systems. *Journal of Hydrology* **543**: 88–100 DOI:

10.1016/j.jhydrol.2016.04.066

Evans C, Davies TD. 1998. Causes of concentration/discharge hysteresis and its potential as a tool for analysis of episode hydrochemistry. *Water Resources Research* **34** (1): 129–137 DOI: 10.1029/97WR01881

Fetter CW. 2013. *Applied Hydrogeology*. Pearson Education Limited: Harlow.

Findlay S. 1995. Importance of surface-subsurface The hyporheic zone exchange in stream ecosystems : *Limnology and Oceanography* **40** (1): 159–164

Gelhar LW, Welty C, Rehfeldt KR. 1992. A critical review of data on field - scale dispersion in aquifers. *Water resources research* **28** (7): 1955-1974

Geuzaine C, Remacle J-F. 2009. Gmsh: A 3-D finite element mesh generator with built-in pre- and post-processing facilities. *International Journal for Numerical Methods in Engineering* **79** (11): 1309–1331 DOI: 10.1002/nme.2579

Gomez JD, Wilson JL. 2013. Age distributions and dynamically changing hydrologic systems: Exploring topography-driven flow. *Water Resources Research* **49** (3): 1503–1522 DOI: 10.1002/wrcr.20127

Gomez JD, Wilson JL, Cardenas MB. 2012. Residence time distributions in sinuosity-driven hyporheic zones and their biogeochemical effects. *Water Resources Research* **48** (9):W09533 DOI: 10.1029/2012WR012180

Hester ET, Cardenas MB, Haggerty R, Apte S V. 2017. The importance and challenge of hyporheic mixing. *Water Resources Research* **53** (5): 3565–3575 DOI: 10.1002/2016WR020005

Hester ET, Young KI, Widdowson MA. 2013. Mixing of surface and groundwater induced by riverbed dunes: Implications for hyporheic zone definitions and pollutant reactions.

Water Resources Research **49** (9): 5221–5237 DOI: 10.1002/wrcr.20399

Horvatic D, Stanley H, Podobnik B. 2011. Detrended cross-correlation analysis for non-stationary time series with periodic trends. *EPL (Europhysics Letters)* **94**

Hucks-Sawyer A, Bayani Cardenas M, Bomar A, Mackey M. 2009. Impact of dam operations on hyporheic exchange in the riparian zone of a regulated river. *Hydrological Processes* **23** (15): 2129–2137 DOI: 10.1002/hyp.7324

Kirchner JW. 2003. A double paradox in catchment hydrology and geochemistry.

Hydrological Processes **17** (4): 871–874 DOI: 10.1002/hyp.5108

Kolditz O, Bauer S, Bilke L, Boettcher N, Delfs JO, Fischer T, Goerke UJ, Kalbacher T,

Kosakowski G, McDermott CI, et al. 2012. OpenGeoSys: An open-source initiative for numerical simulation of thermo-hydro-mechanical/chemical (THM/C) processes in porous media. *Environmental Earth Sciences* **67** (2): 589–599 DOI: 10.1007/s12665-012-1546-x

Krein A, De Sutter R. 2001. Use of artificial flood events to demonstrate the invalidity of

simple mixing models. *Hydrological sciences journal* **46** (4): 611–622 Kresic N. 1997.

Hydrogeology and Groundwater Modeling. CRC Press: New York Liao Z, Osenbrück K,

Cirpka OA. 2014. Non-stationary nonparametric inference of river-to-groundwater

travel-time distributions. *Journal of Hydrology* **519**: 3386–3399 DOI:

10.1016/j.jhydrol.2014.09.084

McCallum JL, Shanafield M. 2016. Residence times of stream-groundwater exchanges due to

transient stream stage fluctuations. *Water Resources Research* **52** (3): 2059–2073 DOI:

10.1002/2015WR017441

Nixdorf E, Sun Y, Lin M, Kolditz O. 2017. Development and application of a novel method for regional assessment of groundwater contamination risk in the Songhua River Basin.

Science of the Total Environment **605–606** DOI: 10.1016/j.scitotenv.2017.06.126

Osenbrück K, Wöhling T, Lemke D, Rohrbach N, Schwientek M, Leven C, Castillo Alvarez C, Taubald H, Cirpka OA. 2013. Assessing hyporheic exchange and associated travel times by hydraulic, chemical, and isotopic monitoring at the Steinlach Test Site,

Germany. *Environmental Earth Sciences* **69** (2): 359–372 DOI: 10.1007/s12665-012-2155-4

Pinay G, O’Keefe TC, Edwards RT, Naiman RJ. 2009. Nitrate removal in the hyporheic zone of a salmon river in Alaska. *River Research and Applications* **25** (4): 367–375 DOI:

10.1002/rra.1164

Ray C. 2008. Worldwide potential of riverbank filtration. *Clean Technologies and*

Environmental Policy **10** (3): 223–225 DOI: 10.1007/s10098-008-0164-5

Razavi S, Elshorbagy A, Wheater H, Sauchyn D. 2015. Toward understanding

nonstationarity in climate and hydrology through tree ring proxy records. *Water*

Resources Research **51** (3): 1813–1830

Sandén P, Karlsson S, Düker A, Ledin A, Lundman L. 1997. Variations in hydrochemistry, trace metal concentration and transport during a rain storm event in a small catchment.

Journal of Geochemical Exploration **58** (2–3): 145–155 DOI: 10.1016/S0375-

6742(96)00078-7

Sawyer, A.H., Cardenas, M.B., Bomar, A., Mackey, M., 2009. Impact of dam operations on

hyporheic exchange in the riparian zone of a regulated river 2137, 2129–2137.

doi:10.1002/hyp

Schmidt C, Bayer-Raich M, Schirmer M. 2006. Characterization of spatial heterogeneity of groundwater-stream water interactions using multiple depth streambed temperature measurements at the reach scale. *Hydrology and Earth System Sciences Discussions* **3** (4): 1419–1446 DOI: 10.5194/hessd-3-1419-2006

Schmidt C, Musolff A, Trauth N, Vieweg M, Fleckenstein JH. 2012. Transient analysis of fluctuations of electrical conductivity as tracer in the stream bed: 3689–3697 DOI: 10.5194/hess-16-3689-2012

Sheets R a., Darner R a., Whitteberry BL. 2002. Lag times of bank filtration at a well field, Cincinnati, Ohio, USA. *Journal of Hydrology* **266** (3–4): 162–174 DOI: 10.1016/S0022-1694(02)00164-6

Sun F, Shao H, Wang W, Watanabe N, Bilke L, Yang Z, Huang Z, Kolditz O. 2012. Groundwater deterioration in Nankou—a suburban area of Beijing: data assessment and remediation scenarios. *Environmental Earth Sciences* **67** (6): 1573–1586 DOI: 10.1007/s12665-012-1600-8

Trauth N, Fleckenstein JH. 2017. Single discharge events increase reactive efficiency of the hyporheic zone. *Water Resources Research* **53** (1): 779–798 DOI: 10.1002/2016WR019488

Trauth N, Schmidt C, Maier U, Vieweg M, Fleckenstein JH. 2013. Coupled 3-D stream flow and hyporheic flow model under varying stream and ambient groundwater flow conditions in a pool-riffle system. **49**: 5834–5850 DOI: 10.1002/wrcr.20442

Trauth N, Schmidt C, Vieweg M, Oswald SE, Fleckenstein JH. 2015. Hydraulic controls of in-stream gravel bar hyporheic exchange and reactions. *Water Resources Research* **51** (4): 2243–2263 DOI: 10.1002/2014WR015857

Vidon P. 2012. Towards a better understanding of riparian zone water table response to precipitation: Surface water infiltration, hillslope contribution or pressure wave processes? *Hydrological Processes* **26** (21): 3207–3215 DOI: 10.1002/hyp.8258

Vieweg M, Kurz MJ, Trauth N, Fleckenstein JH, Musolff A, Schmidt C. 2016. Estimating time-variable aerobic respiration in the streambed by combining electrical conductivity and dissolved oxygen time-series. *Journal of Geophysical Research: Biogeosciences* DOI: 10.1002/2016JG003345

Vogt T, Hoehn Dr. E, Schneider Dr. P, Cirpka Dr. OA. 2009. Untersuchung der flusswasserinfiltration in voralpinen schottern mittels Zeitreihenanalyse. *Grundwasser* **14** (3): 179–194 DOI: 10.1007/s00767-009-0108-y

Vogt T, Hoehn E, Schneider P, Freund A, Schirmer M, Cirpka O a. 2010. Fluctuations of electrical conductivity as a natural tracer for bank filtration in a losing stream. *Advances in Water Resources* **33** (11): 1296–1308 DOI: 10.1016/j.advwatres.2010.02.007

Welch, C., Cook, P.G., Harrington, G.A., Robinson, N.I., 2013. Propagation of solutes and pressure into aquifers following river stage rise. *Water Resour. Res.* 49, 5246–5259. doi:10.1002/wrcr.20408

Welch, C., Harrington, G.A., Leblanc, M., Batlle-Aguilar, J., Cook, P.G., 2014. Relative rates of solute and pressure propagation into heterogeneous alluvial aquifers following river flow events. *J. Hydrol.* 511, 891–903. doi:10.1016/j.jhydrol.2014.02.032

Wollschläger U, Attinger S, Borchardt D, Brauns M, Cuntz M, Dietrich P, Fleckenstein JH,

Friese K, Friesen J, Harpke A, et al. 2017. The Bode hydrological observatory: a platform for integrated, interdisciplinary hydro-ecological research within the TERENO

Harz/Central German Lowland Observatory. *Environmental Earth Sciences* **76** (1) DOI:

10.1007/s12665-016-6327-5

Zarnetske JP, Haggerty R, Wondzell SM, Bokil V a., González-Pinzón R. 2012. Coupled

transport and reaction kinetics control the nitrate source-sink function of hyporheic

zones. *Water Resources Research* **48** (11): W11508 DOI: 10.1029/2012WR011894

Accepted Article

Table 1: Parameterization of the OpenGeoSys groundwater flow model. The parameters written in *italic* were determined during the model calibration procedure.

River configuration	
River slope	0.2-1.8 %
River width	7 m
River length	350 m
Domain configuration	
Domain width/length	325/325 m
Mesh cell resolution	0.3-19.5 m
Number of elements	36509
Subsurface configuration	
Porosity	0.3
<i>Hydraulic conductivity</i>	<i>1.28*10⁻³ m/s</i>
<i>Depth to Groundwater at Q_{min}</i>	<i>2.91 m</i>
<i>Depth to Groundwater at Q_{max}</i>	<i>1.87 m</i>

Table 2: Calculated advective travel time τ and corresponding correlation coefficient ρ for 16 water-mill-induced EC fluctuations in well F4.

Event No.	τ [h]	ρ [-]
1	3.2	0.80
2	3	0.65
3	2.7	0.64
4	3	0.61
5	2.5	0.86
6	3	0.60
7	2.3	0.80
8	3.3	0.88
9	3.5	0.71
10	2.7	0.86
11	1.2	0.74
12	2.7	0.83
13	3.3	0.93
14	2.8	0.64
15	2.7	0.88
16	1	0.79
Mean \pm std.	2.7 \pm 0.70	0.76 \pm 0.11

Table 3: Calculated travel times and corresponding correlation coefficient ρ derived by windowed cross-correlation for the storm events. Please note that the negative travel times were omitted for calculating the average values.

Event No.	F1		F2		F3		F4	
	τ [h]	ρ [-]	τ [h]	ρ [-]	τ [h]	ρ [-]	τ [h]	ρ [-]
#1	-	-	18.8	0.41	-2.3	0.64	-1.5	0.84
#2	-	-	12.2	0.27	-1.8	0.80	-5.5	0.85
#3	1.8	0.05	41.3	0.45	-34.2	0.86	-5.8	0.93
#4	-	-	21.7	0.48	-3.2	0.65	2.2	0.52
#5	-	-	16.7	0.08	-15.5	0.97	-7.7	0.86
#6	-	-	1.5	0.63	24.2	0.41	5.2	0.43
#7	-	-	0.7	0.57	29.7	0.41	-11	-0.02
#8	-	-	7.8	0.68	-5.8	0.60	1.2	0.93
Mean \pm std.	1.8	0.05	15.1 \pm 13.11	0.45 \pm 0.19	26.9 \pm 3.89	0.41	2.8 \pm 2.08	0.63 \pm 0.26

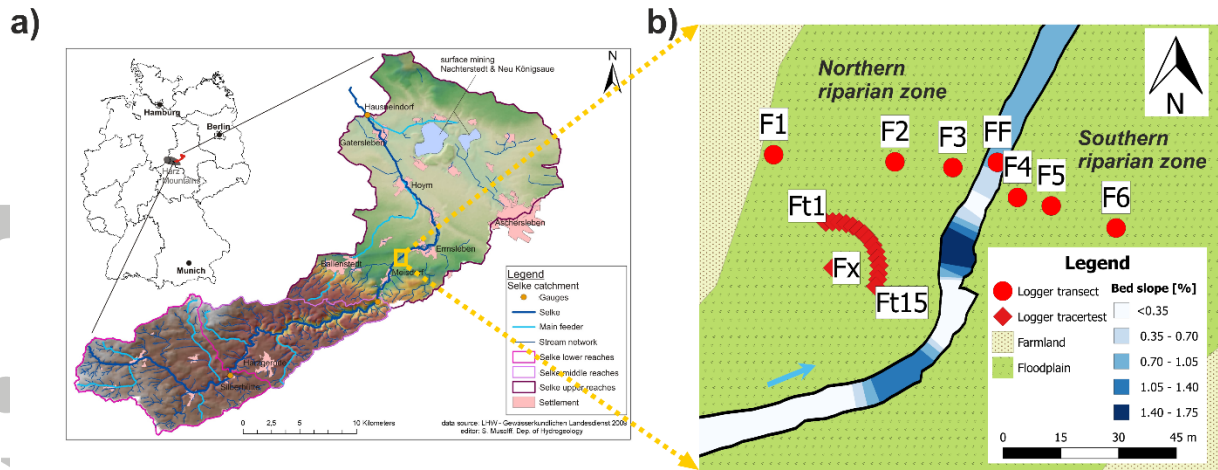


Figure 1: a) Location of the Selke intensive research site (yellow rectangle) within the Selke catchment in Germany. b) Detailed view on the location of the groundwater monitoring wells and the river water observation (“FF”). The colour of the river line represents the slope of the river water level, which varies due to pronounced pool-riffle sequences. The light blue arrow visualises the flow direction of the Selke River.

Accepted Article

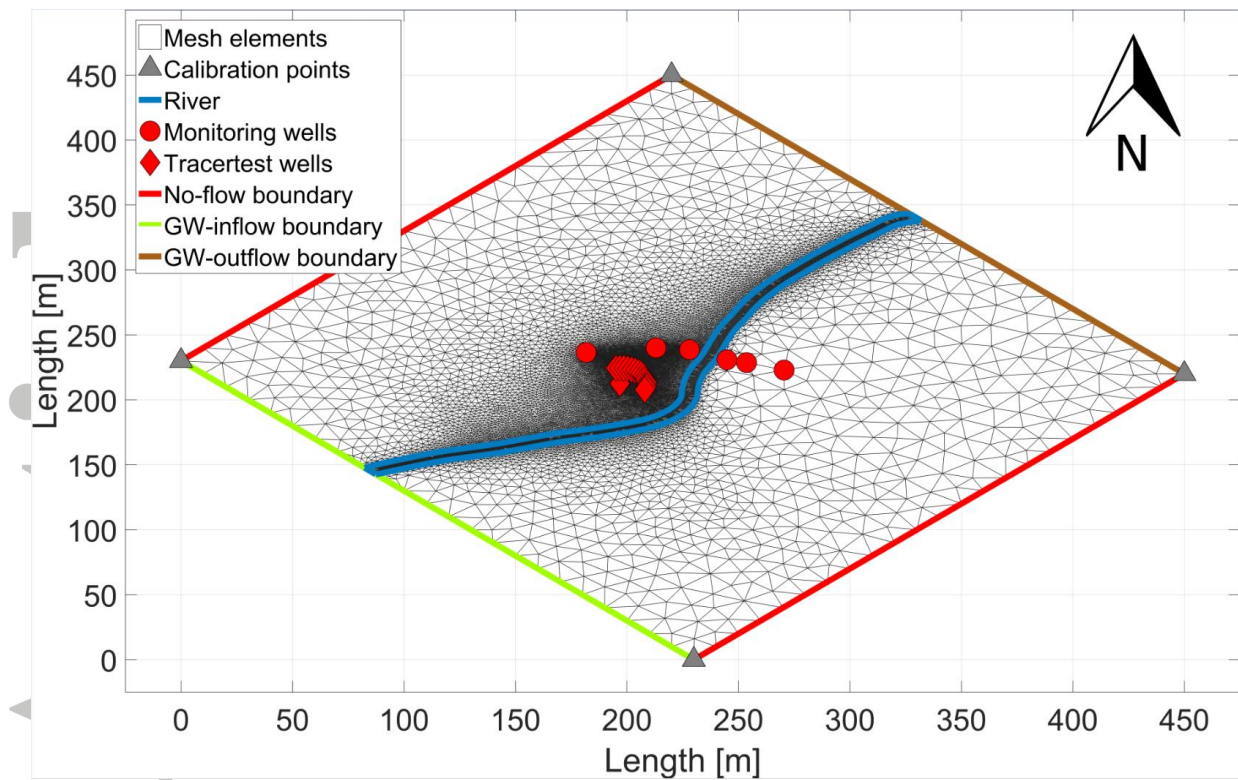


Figure 2: Configuration of the numerical groundwater flow model including the mesh (grey triangles), the representative river area (blue lines) and the location of the groundwater boundary condition (green and brown lines) and calibration points (grey triangles).

Accepted

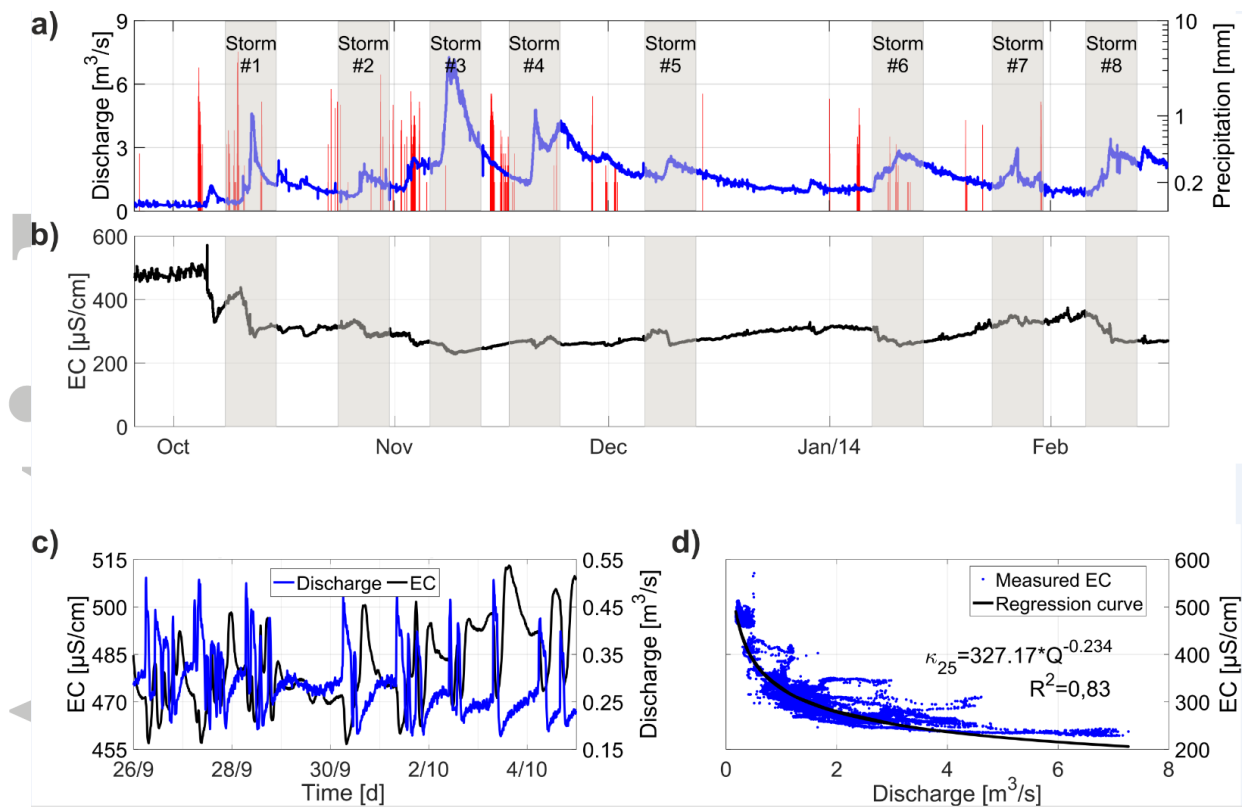


Figure 3: Characteristics of water level and electrical conductivity in the Selke River. a) and b) Time series of discharge and EC in the Selke River at the study site. The red bars show the precipitation measured at the local weather station. The grey boxes highlight the eight storm events which were used for cross-correlation analysis. c) EC and discharge during the period of water-mill operations. d) Relationship between EC and river discharge including the best-fitting curve.

Accepted

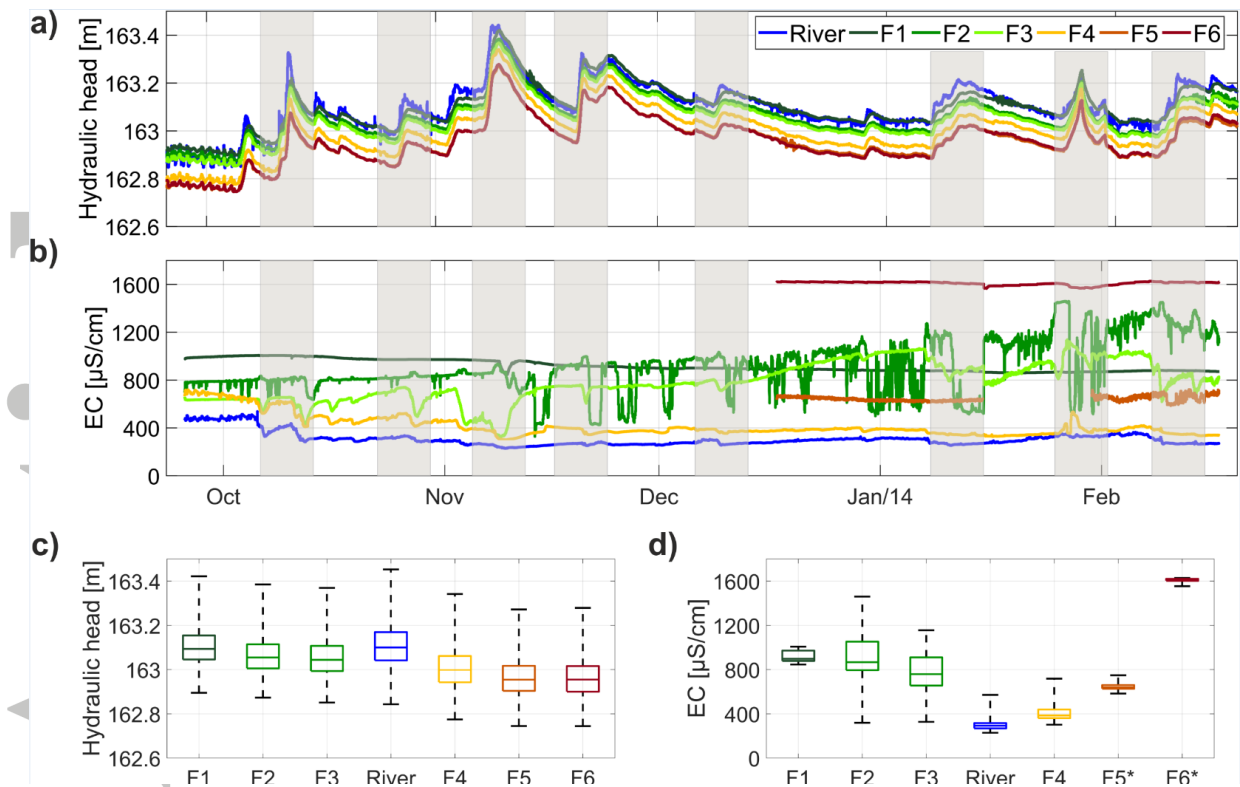


Figure 4: Spatial-temporal distribution of hydraulic heads and EC at the study site. a) and b) Time series of hydraulic head and EC for the entire monitoring period. For visualisation purposes, the curves were smoothed by using a moving average filter with a filter window of five time steps (50 minutes). The grey boxes highlight the eight storm events which were used for cross-correlation analysis. c) and d) Spatial distribution of mean hydraulic heads and EC along the transect. The * at the EC bars of the wells F5 and F6 indicates the shorter length of the available time series. The whiskers in the boxplot correspond to the entire spectrum of measured values at each well.

Accepted

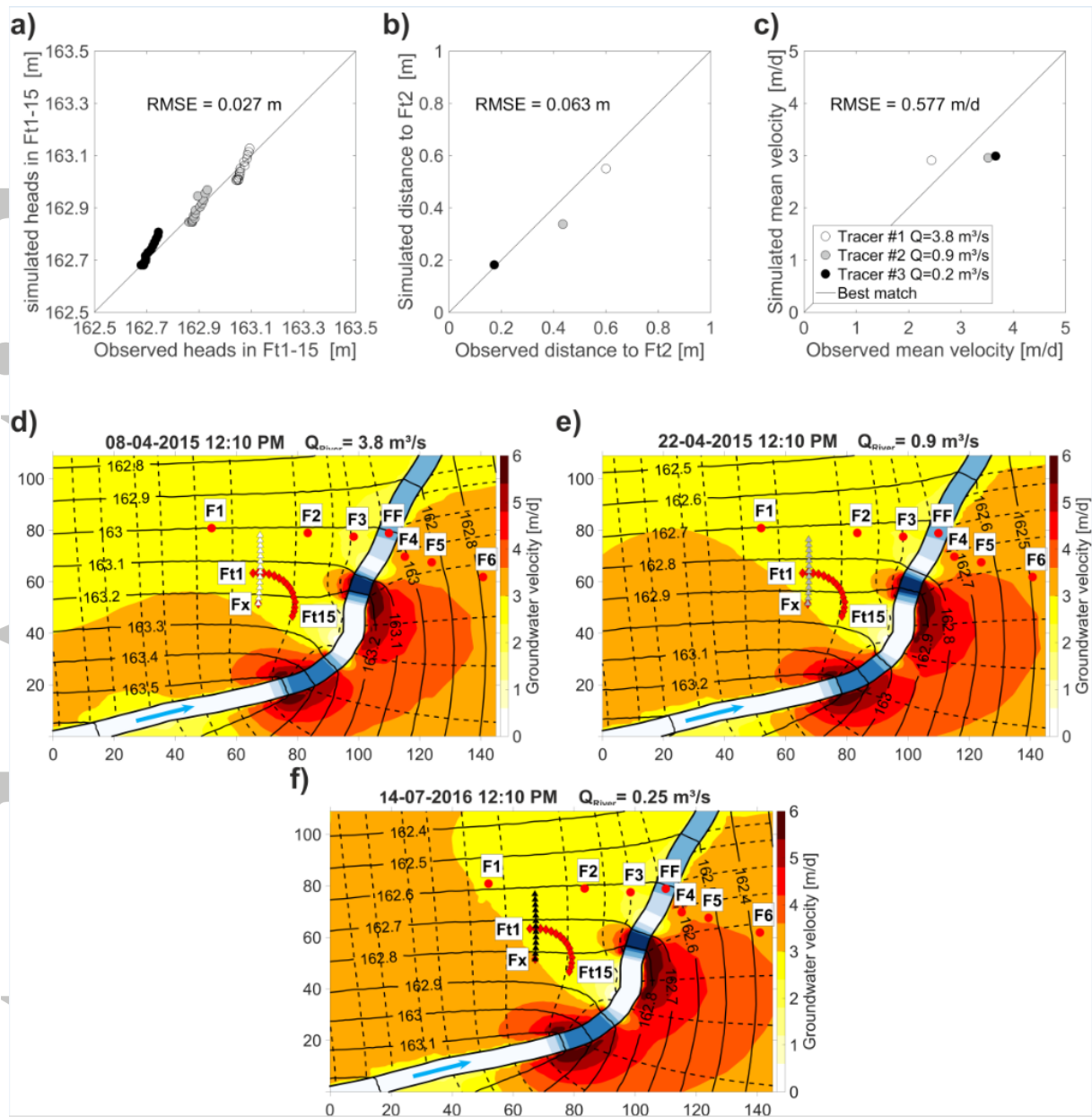


Figure 5: Simulated subsurface flow field characteristics during the salt tracer tests. a-c) Comparison between observed and simulated hydraulic heads, location of the tracer breakthrough and mean tracer velocity of each tracer test. The latter parameter was obtained from the calibrated mean advective tracer travel time and the distance from the injection well. Line shows the 1:1 relationship and the given RMSE evaluates the performance of the calibrated simulation. d-f) Calculated flow field for the injection time of each tracer test. The simulated particle tracks are visualised by the greyish triangles. Hydraulic heads are shown as solid black lines and stationary flow paths as dashed lines. The colouring of the river corridor refers to the different slopes (see Fig. 1c). Axis labelling shows distances in meters from the local coordinate origin.

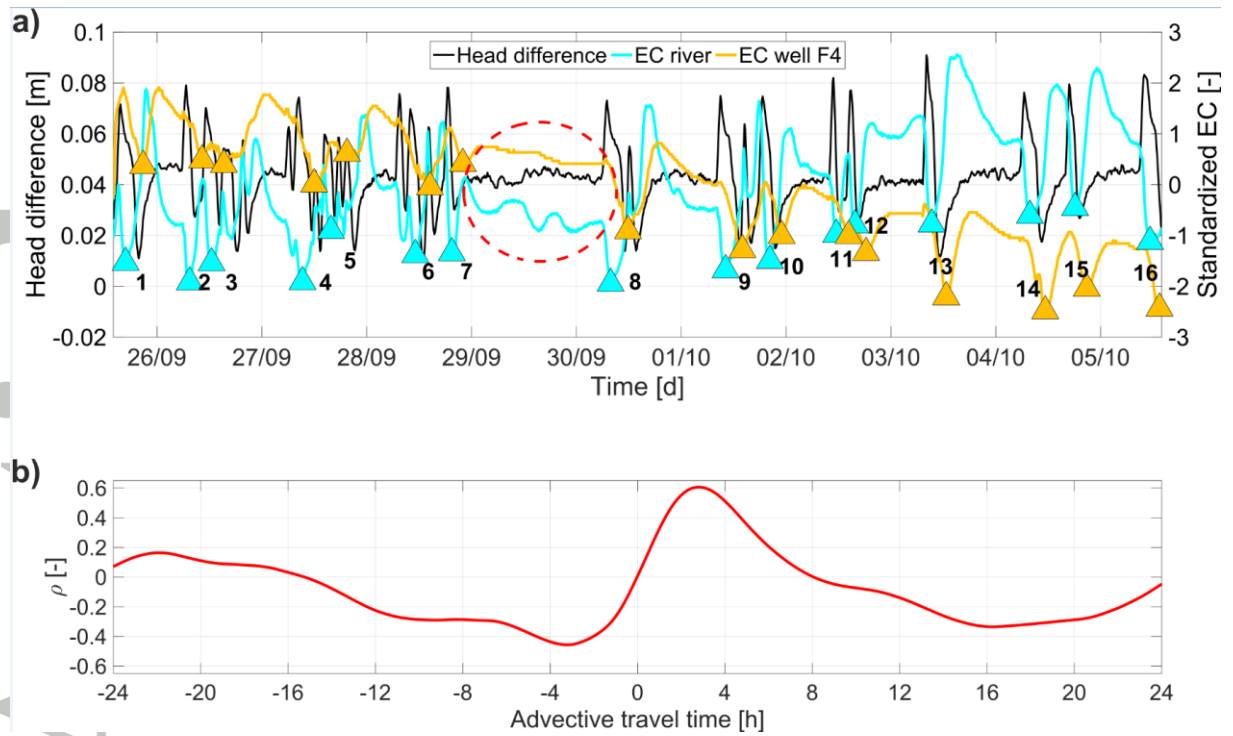


Figure 6: Propagation of mill-induced river EC fluctuation to monitoring well F4. a) EC time series of river and well F4 and head differences. The red circle indicates a day in which the mill was not operational and EC fluctuations were absent in well F4. b) Dependence of the cross-correlation coefficient on the number of shifted time steps for the entire time series.

Accepted

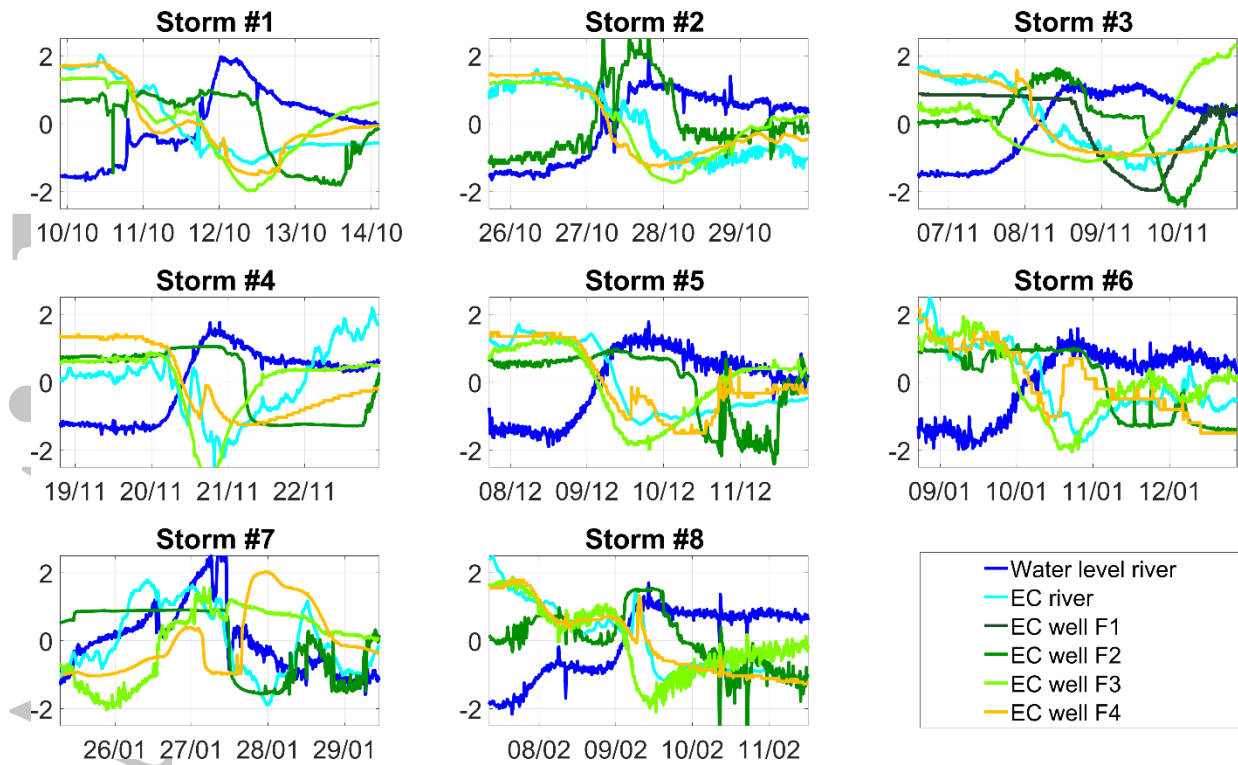


Figure 7: Propagation of EC breakthrough curves for individual storm events. Each subplot shows a window of 300 time steps (50 hours) backward and forward from the measured stage peak of each storm event. The storm event numbers correspond to the grey boxes in Figure 2. River stage and EC signals are shown as detrended time series

Accepted

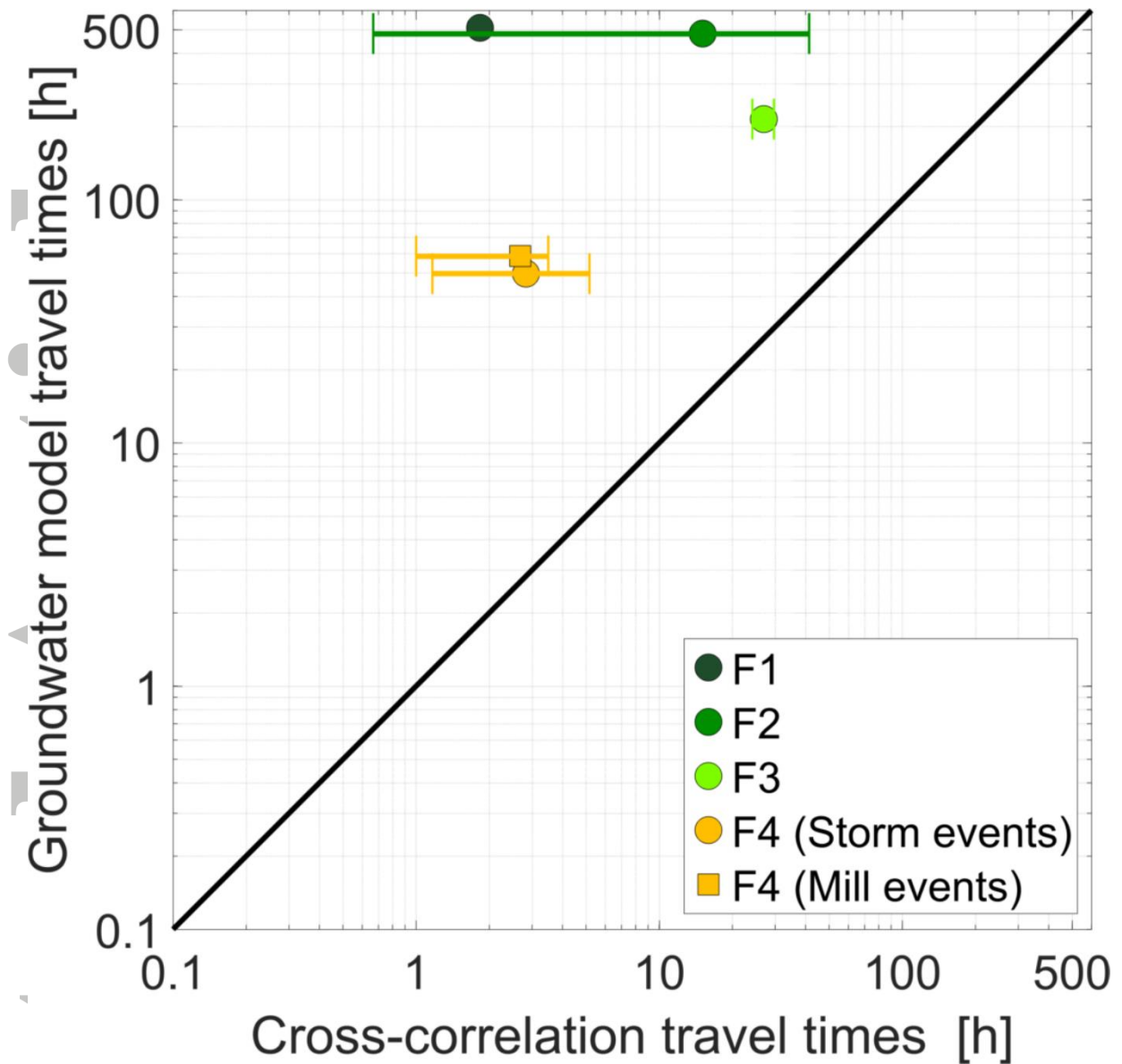


Figure 8: Comparison of mean subsurface travel times estimated by the groundwater flow model and the cross-correlation analysis. The whiskers in the boxplot correspond to the entire spectrum of estimated positive cross-correlation estimates at each well. The range of groundwater model estimates was smaller than the size of the markers and is thus not displayed in the graph.

Accepted

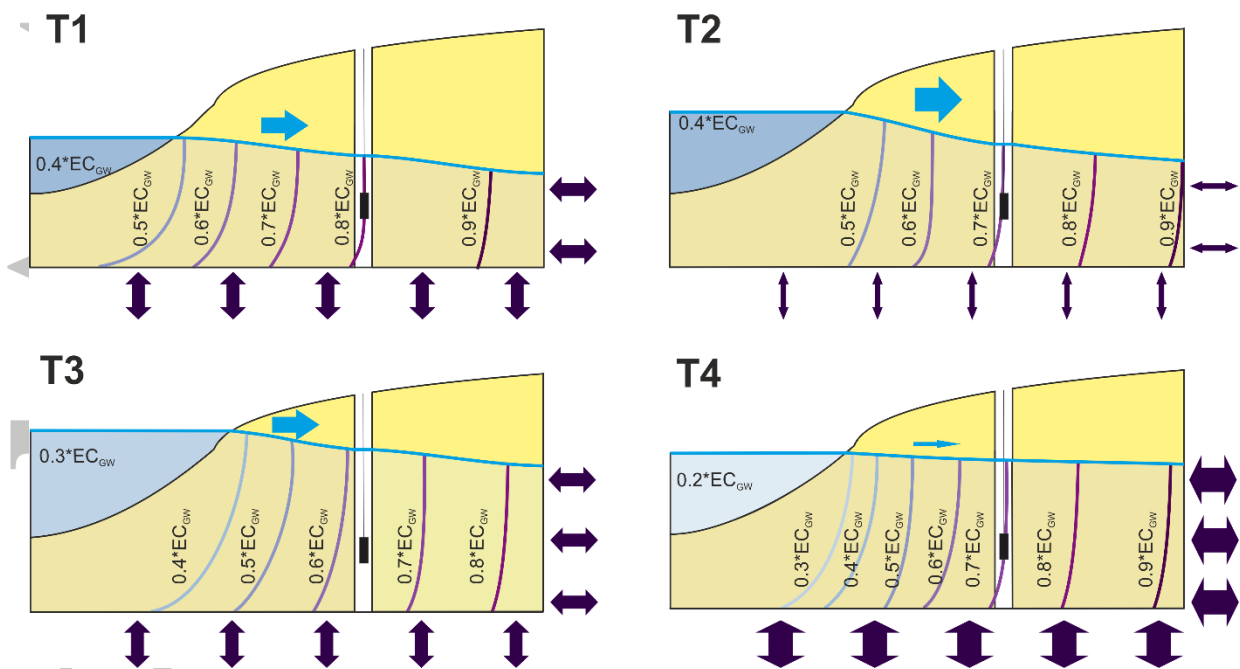
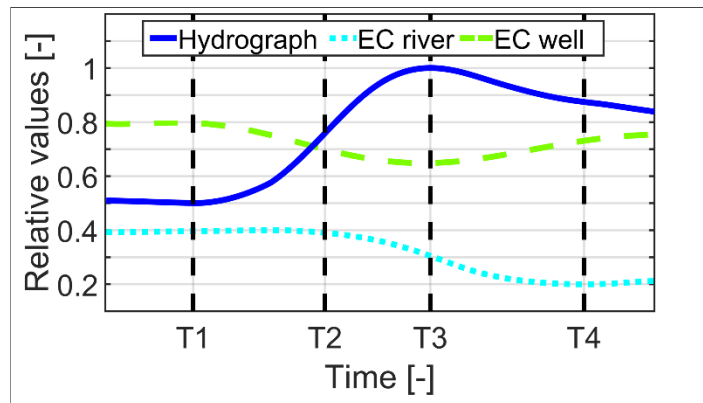


Figure 9: Conception of the development of bank-storage-driven EC breakthrough curves in a monitoring well under losing conditions. The upper plot shows an idealized form of EC propagation during an event where the letters on the x-axis refer to the lower pictures in chronological order from time T1 to T4. The width of the dark purple double-arrows visualises the magnitude of ambient groundwater impact and the width of the horizontal light blue arrow in each subplot indicates the magnitude of losing conditions in the riparian zone during a storm event. T1) EC distribution prior to an event as the result of continuous mixing processes in the riparian aquifer. T2) The increasing river stage pushes low-EC riparian water into the monitoring well, but river EC remains constant. T3) At peak water level, river EC is declining but weakened hydraulic gradients are slowing the EC decrease in the monitoring well. T4) On the falling limb of the storm event, river EC reaches its minimum. However, stronger groundwater impact due to weak losing conditions inhibits a further decline of EC in the monitoring well and a subsequent recovery of EC can be observed.

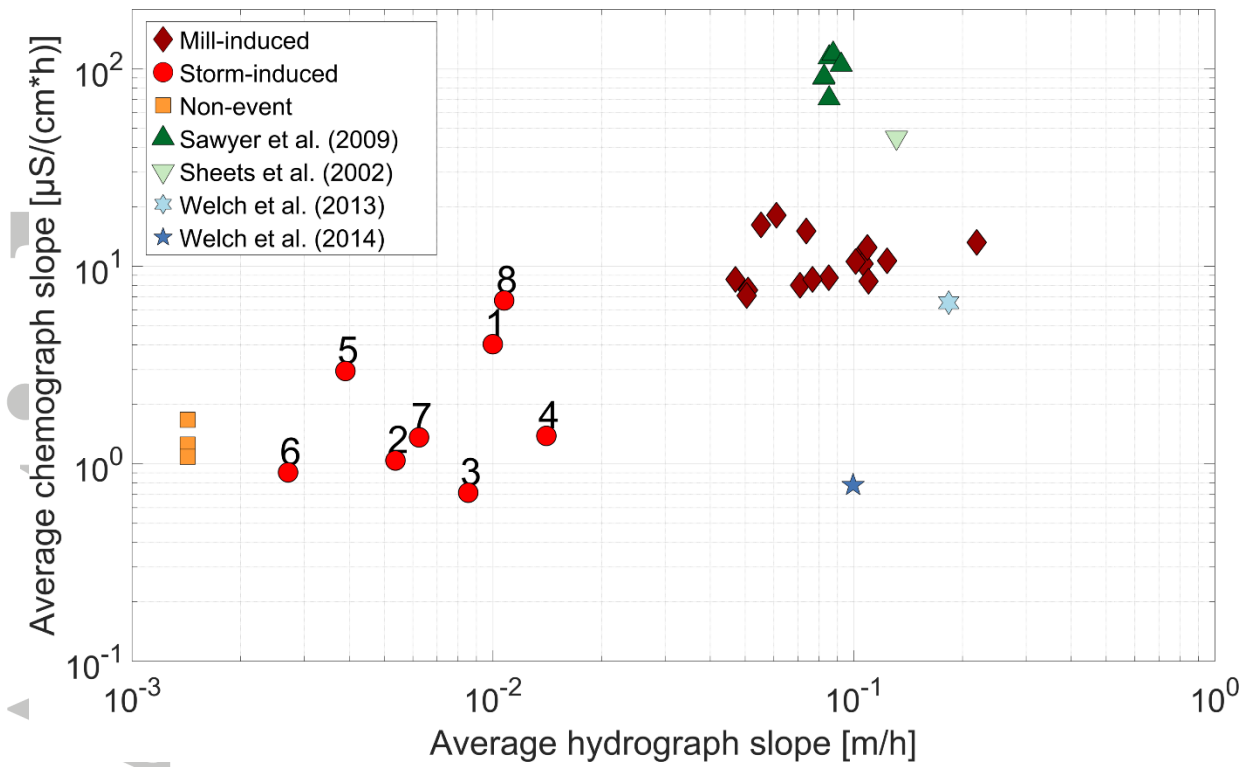


Figure 10: Characterisation of different events by the average slope of the rising river hydrograph and the corresponding falling EC signal. The term non-event refers to the EC fluctuations in the river on 29th of September 2013.

Accepted